Petroleum Science 23 (2026) 2120–2135

Contents lists available at ScienceDirect

Petroleum Science

journal homepage: www.keaipublishing.com/en/journals/petroleum-science

Original Paper

Three-dimensional heat transfer model of oil-water two-phase stratified flow

Hui-Shu Liu [a], Ji-Miao Duan [b,*], Yong-Xiang Huang [b], Hao-Nan Li [b], Shuo Xu [b], Shi-Ming Chen [b], Hui-Rong Huang [a]

[a] School of Petroleum Engineering, Chongqing University of Science and Technology, Chongqing, 401331, China
[b] PLA Joint Logistics Support Force University of Engineering, Chongqing, 401331, China

ARTICLE INFO

Article history:
Received 7 August 2025
Received in revised form
24 October 2025
Accepted 5 December 2025
Available online 10 December 2025

Edited by Teng Zhu

Keywords:
Oil-water two-phase flow
Stratified flow
Heat transfer characteristics
Numerical model

ABSTRACT

Oil-water stratified flow, a fundamental pattern in multiphase pipe flow, is commonly encountered in offshore petroleum production and transportation. Although hydraulic characteristics of this flow regime have been extensively studied, accurate prediction of its heat transfer behavior under non-isothermal conditions remains a challenge. In this study, we develop a three-dimensional heat transfer model for oil-water stratified flow by integrating the energy conservation equation with established flow models and coupling it with momentum conservation. Turbulence is resolved using a low-Reynolds-number k-ε model. The phase interface is captured via a minimum energy model, and the irregular physical domain is transformed into a regular rectangular region using bipolar coordinates to simplify grid generation and numerical solution. The model was validated against experimental measurements of average outlet temperatures for both phases, showing relative errors within 5%. Results further reveal how water cut influences the axial temperature distribution and highlight three-dimensional temperature profiles during non-isothermal flow. This model provides theoretical insights and practical tools for optimizing thermal management and ensuring safety in offshore petroleum pipeline operations.

1. Introducion

With the advancement of deep-water and ultra-deep-water drilling in oilfield operations, the presence of water in crude oil pipelines has become more common (Zhang et al., 2024; Yin et al., 2025). During late-stage oilfield development, declining reservoir pressure commonly necessitates water injection for enhanced recovery, leading to the ubiquity of oil-water two-phase pipe flow in crude oil production and transportation systems (Chen et al., 2025). Stratified flow is a typical pattern in such two-phase pipe flows and serves as the foundation for analyzing other flow patterns (Li and Chen, 2024; Małgorzata et al., 2024). Consequently, investigating the heat transfer characteristics of oil-water stratified flow under deep-water and low-temperature conditions holds significant engineering value for deep-water oil and gas resource development and ensuring pipeline safety.

While significant research has been conducted on oil-water two-phase flow, most efforts have been concentrated on hydrodynamic characteristics, leaving the heat transfer aspects relatively underexplored (Cezary and Paweł, 2024; Sunday et al., 2023). Research on heat transfer in multiphase flow has primarily targeted gas-liquid two-phase flow, supported by extensive experimental and modeling studies (Jia and Dong, 2023; Yang et al., 2023). However, significant differences exist between oil-water and gas-liquid two-phase flows, particularly in their density and viscosity ratios, interfacial free energy, momentum transfer characteristics, and phase interface evolution mechanisms. Therefore, the gas-liquid flow heat transfer model cannot be directly applied to the study of oil-water two-phase flow.

Somer et al. (1973) developed a model for the heat transfer coefficient in oil-water flow and found that the predictions remained within ±15% error for oil volume fractions below 50% and Reynolds numbers under 20×10^4. Lang and Auracher (1996)

* Corresponding author.
E-mail address: duanjimiao@126.com (J.-M. Duan).
Peer review under the responsibility of China University of Petroleum (Beijing).

https://doi.org/10.1016/j.petsci.2025.12.012

examined vertical *n*-heptane-water flow and noted a marked change in heat transfer beyond 50% *n*-heptane fraction. They proposed a linear mixing model based on volume fraction, though linear interpolation led to considerable prediction errors. Similarly, Hapanowicz and Polaczek (2013) also found that during the flow of two immiscible liquids in the pipeline, unless the liquid-liquid flow system is uniformly mixed, the heat transfer coefficient calculation error of heterogeneous flow will reach 35%–45%. Building upon prior dispersion studies, Karimi and Boostani (2016) systematically studied oil-water heat transfer in horizontal pipelines and developed predictive models for laminar, oil-in-water (O/W), and water-in-oil (W/O) dispersed flows based on flow patterns, with predictions within ±20% of experimental data. Piroozian et al. (2016) established a temperature model for waxy oil-water flow near wax precipitation points, incorporating the latent heat of wax precipitation into the specific heat capacity of crude oil. Hong et al. (2025) established a mathematical model of multiphase flow in vertical wellbores under high gas and liquid conditions. Through verification with actual data, the model error was controlled within 5%, and based on this, the variation characteristics of pressure drop at the transition boundary of different flow patterns were explained.

The aforementioned heat transfer calculation models for liquid-liquid two-phase flow all assume identical axial temperature gradients for both phases. However, this assumption is only valid for dispersed flows (e.g., O/W or W/O emulsions) and leads to substantial errors when applied to stratified or interfacial mixing flows. To address this limitation, Shang and Sarica (2013) developed a temperature distribution model based on energy balance within control volumes for stratified oil-water flow. The model was validated against single-phase heat transfer correlations at 0% and 100% water cut, and experimentally at 50% water cut. Results from both modeling and experiments show that water cut critically influences heat transfer: the temperature difference between oil and water phases increases downstream from the inlet and gradually decreases after a certain flow length.

Research on stratified flow in oil-water systems is extensive, yet studies on its heat transfer behavior remain scarce. Most existing heat transfer models for such flows are one-dimensional and rely on empirical correlations to close the energy equation, especially under turbulent conditions. These approaches often lead to significant errors and are inadequate for predicting temperature fields in pipelines affected by wax deposition. To overcome these limitations, researchers have increasingly turned to computational fluid dynamics (CFD) in recent years to investigate heat transfer in oil-water two-phase flow.

Li et al. (2015a, b) developed a numerical model for three-phase stratified flow and heat transfer between parallel plates. Using the Level Set method for interface tracking and the finite volume method to solve the coupled governing equations, they validated the model against the exact solution for single-phase flow under constant wall temperature. Subsequently, the study examined the influence of Weber number (We), Froude number (Fr), fluid velocity, viscosity, and thermal conductivity on the velocity and temperature fields. Models were also established for local Nusselt number (Nu_x) and fully developed Nusselt numbers (Nu_f). Results showed that increasing the flow rates of both bottom and top fluids enhanced the upper and lower wall Nusselt numbers at the upper wall (Nu_{fu}) and lower wall Nusselt number (Nu_{fl}). In contrast, higher viscosity and thermal conductivity in the bottom fluid increased Nu_{fu} but decreased Nu_{fl}, while increasing these properties in the top fluid had the opposite effect.

Garmroodi and Ahmadpour (2020) conducted a three-dimensional numerical simulation of stratified waxy crude oil-water flow in a horizontal pipe. The results indicated high sensitivity of pressure drop on wax content. Increasing the wax content from 3.2% to 5.5% led to a 117% rise in pressure drop, whereas applying a uniform wall heat flux reduced it by 25%. Despite these insights into global parameters, the study lacked detailed analysis of the velocity fields of oil and water, wall shear stress distribution, or temperature field characteristics. In contrast, Li et al. (2018) developed a quasi-three-dimensional heat transfer model for waxy oil-water stratified wavy flow. The model employed Large Eddy Simulation (LES) to compute turbulent flow and heat transfer in both oil and water phases, utilizing an effective displacement distance ($\triangle y$) to account for the influence of interfacial wave-induced turbulence. Moreover, detailed analysis was conducted on temperature and velocity distributions across various pipe cross-sections. Nevertheless, the calculated results for the pipe wall temperature field were not validated against experimental or numerical benchmarks.

Conventional models for oil-water two-phase flow and heat transfer are typically one-dimensional, assuming constant physical properties and thermo-hydraulic parameters over the pipe cross-section. As a result, they neglect variations in hydraulic and thermal parameters within the fluid and along the pipe wall circumference, particularly the distributions of shear stress and temperature. To address these limitations, we developed a stratified flow heat transfer model by integrating an energy equation with existing flow models coupled to momentum conservation. This model was used to analyze the effect of water cut on the axial temperature distribution of both phases and reveal three-dimensional temperature profiles during non-isothermal stratified flow. The results provide theoretical support for offshore petroleum production and pipeline transport.

2. Control equations

To determine the temperature distribution of the oil and water phases within a pipeline cross-section, it is essential to formulate both the momentum transfer equation and the energy transfer equation. Correspondingly, specific flow and heat transfer boundary conditions must be defined based on the actual flow and heat transfer conditions. Under non-isothermal heat transfer conditions, momentum and heat transfer occur between the oil phase and the environment, as well as between the water phase and the environment, as depicted in Fig. 1. Under fully developed steady-state flow conditions, waxy oil and water at constant temperature flow through the pipeline, while the external pipe surface is cooled by a fluid at temperature $T = const$.

In Fig. 1, x, ξ and η represent the three coordinate axes of the coordinate system in meters; u_O and u_W are the axial velocities of the oil phase and water phase, respectively, m/s; τ_I, τ_O and τ_W are the shear stresses at the oil-water interface, oil phase and pipe wall, and water phase and pipe wall, respectively, Pa. Under steady flow conditions, the pressure gradients of the oil phase and water phase are the same, and this pressure gradient balances the sum of the wall shear forces τ_O and τ_W in the water and oil phases. h_e is the coefficient of convective heat transfer outside the pipe (in W/(m^2·K)); T_∞ is the coolant temperature. $q_{int,\ W}$ and $q_{int,\ O}$ are the heat exchanged at the interface of the water and oil phases, respectively (in W/m^2).

When developing a flow and heat transfer calculation model for oil-water two-phase stratified flow, the interface between the oil and water phases in the pipe cross-section is conventionally assumed to be planar. However, in immiscible two-phase stratified flow, the interface can take various shapes depending on factors such as the pipeline's geometric dimensions, the proportion of each phase, the physical properties of the fluids (density and interfacial tension), and the wettability of the pipe wall. It can be

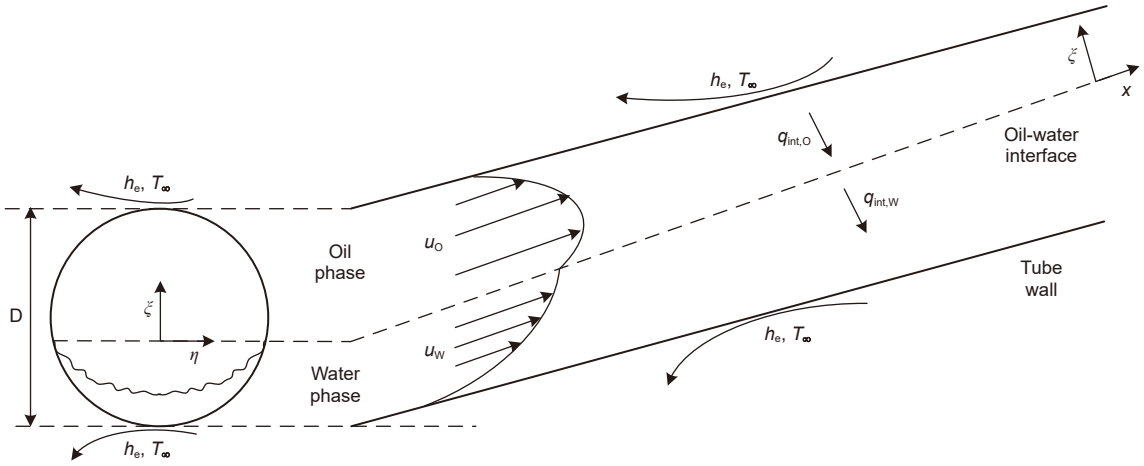

Fig. 1. Schematic diagram of convective heat transfer in fully developed oil-water two-phase stratified flow.

either planar or curved. Recent advances in detection technology have revealed that the oil-water interface in stratified flow typically adopts a curved rather than flat profile. Edomwonyi-Out and Angeli (2015) used an electrical conductivity probe to measure the height of the oil-water interface at the center of the pipe during the stratified flow. The measurements showed a lower interface height at the center compared to the near-wall region, demonstrating a concave interfacial morphology. Santos et al. (2019) used Electrical Impedance Tomography (EIT) to investigate the oil-water interface in a horizontal pipe with waxy oil-water stratified flow, finding a concave interface. This study employs the phase interface minimum energy model proposed by Brauner et al. (1996, 1998) to describe the morphology of the phase interface in oil-water two-phase stratified flow. As depicted in Fig. 2, under the Cartesian coordinate system, the flow regions of both the oil and water phases in the cross-section of the stratified flow pipe are irregular. By using bipolar coordinates, these irregular regions can be transformed into regular rectangular regions, simplifying the network partitioning and numerical solution of the control equations. The details of the oil-water two-phase stratified flow interface model and the application of bipolar coordinates can be found in the previous research results of the research group (Liu et al., 2022).

2.1. Momentum equation

Under steady flow conditions, assuming isotropic turbulence and incompressible fluid in both the oil and water phases, the fully developed flow of the oil and water phases experiences the same pressure gradient. This pressure gradient is balanced by the sum of the wall shear forces τ_O and τ_W in the water and oil phases. In a bipolar coordinate system, the axial momentum equation for each phase in oil-water two-phase stratified flow can be expressed as follows:

$$\frac{1}{l_\eta l_\xi}\frac{\partial}{\partial\xi}\left(\mu_m\frac{\partial u}{\partial\xi}\right)+\frac{1}{l_\eta l_\xi}\frac{\partial}{\partial\eta}\left(\mu_m\frac{\partial u}{\partial\eta}\right)+\frac{1}{l_\xi}\frac{\partial}{\partial\xi}(-\rho\overline{v'u'})+\frac{1}{l_\eta}\frac{\partial}{\partial\eta}(-\rho\overline{w'u'})=\frac{dP}{dx} \quad (1)$$

where u, v and w are the velocity components of the oil or water phase in the axial x, vertical ξ, and circumferential η directions respectively, m/s; dP/dx is the pressure drop gradient in the axial x direction, Pa/m; ρ is the density of the oil or water phase, kg/m^3; μ_m is the molecular viscosity coefficient, m^2/s; $-\rho\overline{v'u'}$, and $-\rho\overline{w'u'}$ are the turbulent additional shear stresses for oil or water phases.

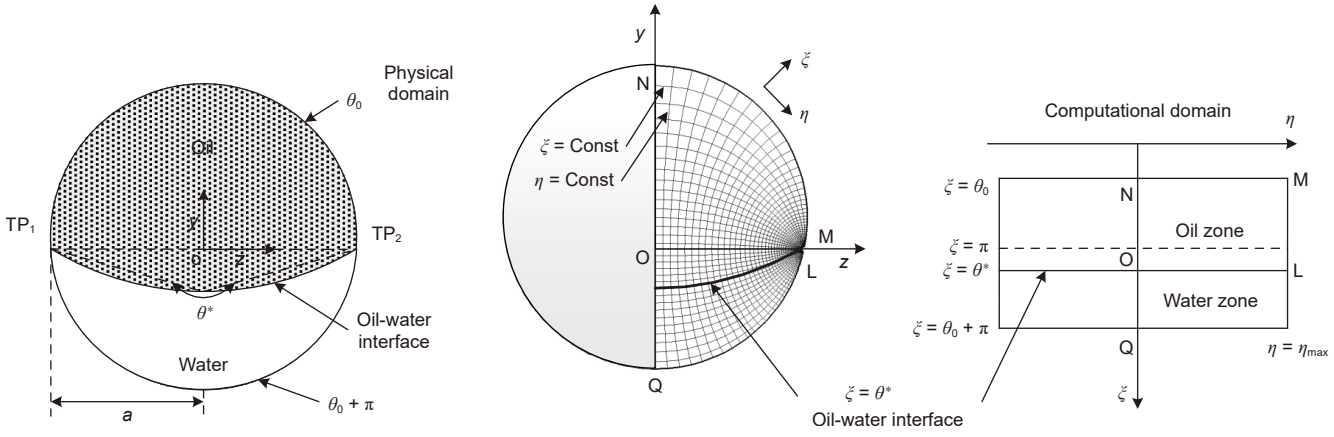

Fig. 2. Calculation region of oil-water two-phase stratified flow in bipolar coordinate system (Liu et al., 2022).

In the dynamically fully developed region, assuming isotropic turbulence and unidirectional flow for both the oil and water phases, the momentum transfer equation can be simplified. For reach phase, the simplified axial momentum equation in a bipolar coordinate system can be written as:

$$\frac{1}{l_\eta l_\xi}\frac{\partial}{\partial \xi}\left(\mu_e \frac{\partial u}{\partial \xi}\right)+\frac{1}{l_\eta l_\xi}\frac{\partial}{\partial \eta}\left(\mu_e \frac{\partial u}{\partial \eta}\right)=\frac{\mathrm{d}P}{\mathrm{d}x} \tag{2}$$

where μ_e is the effective viscosity coefficient, which is the sum of the molecular viscosity coefficient and the turbulent viscosity coefficient, $\mu_e = \mu_m + \mu_t$, m^2/s; μ_t is the turbulent viscosity coefficient of the oil or water phase, m^2/s. Under laminar flow conditions, the turbulent viscosity coefficient $\mu_e = 0$ and the effective viscosity coefficient $\mu_e = \mu_m$.

2.2. Heat transfer equations

The flow temperature is high at the entrance of the oil-water pipeline. While flowing along the pipeline, due to heat transfer with the surroundings, the flow temperature becomes low. It is a fierce convective heat transfer process for the oil-water flow, where the axial heat conductive effect can be neglected. For oil-water two-phase stratified flow, with negligible axial heat conduction and viscous dissipation in the oil and water phases, the energy transfer equations within a bipolar coordinate system are simplified through an approach analogous to that for the momentum equations. The energy equation for fully developed flow of the oil and water phases is given by:

$$\frac{1}{l_\eta l_\xi}\frac{\partial}{\partial \xi}\left[\Gamma_T\left(\frac{\partial T}{\partial \xi}\right)\right]+\frac{1}{l_\eta l_\xi}\frac{\partial}{\partial \eta}\left[\Gamma_T\left(\frac{\partial T}{\partial \eta}\right)\right]=u\frac{\partial T}{\partial x} \tag{3}$$

where T is the temperature of the oil or water phase, °C; Γ_T is the turbulent effective heat diffusion coefficient for oil or water phase, $\Gamma_T = \mu_m/\mathrm{Pr}+\mu_t/\mathrm{Pr}_T$, m^2/s; μ_m is the molecular viscosity coefficient of the oil or water phase, m^2/s; Pr is the Prandtl number, $\mathrm{Pr}=C_p\rho\mu_m/\lambda$; C_P is the specific heat capacity of the oil or water phase, J/kg·K; λ is the thermal conductivity of the oil or water phase, W/(m·K); μ_t is the turbulent viscosity coefficient for oil or water phase, m^2/s; Pr_T is the turbulence Prandtl number.

Jones and Launder (1973) assumed a constant turbulent Prandtl number ($\mathrm{Pr}_T = 0.9$). In contrast, Hishida et al. (1986) demonstrated through experimental studies of turbulent heat transfer in circular pipes that Pr_T remains 0.9 when $d_w^+ > 30$. However, for $d_w^+ < 30$, Pr_T increases significantly toward the pipe wall, reaching 1.6 at $d_w^+ = 10$, where d_w is defined as $d_w{}^+ = (d_w\rho/\mu_m)\sqrt{\tau_W/\rho}$. Kays (1994), based on direct numerical simulation, introduced turbulent viscosity into the turbulent Prandtl number:

$$\mathrm{Pr}_T=\frac{0.7}{\frac{\mu_t}{\mu_m}\mathrm{Pr}}+0.85 \tag{4}$$

2.3. Turbulence equation

During the oil-water two-phase stratified flow process, the flow states in the oil and water phases may be classified into four scenarios: laminar-laminar (L-L), laminar-turbulent (L-T), turbulent-laminar (T-L), or turbulent-turbulent (T-T). Typically, turbulence occurs more readily in the water phase than in the oil phase under identical flow conditions. For turbulence flow, the k-ε model, which couples the turbulent kinetic energy k with the turbulent dissipation rate ε, is used to describe the turbulence characteristics. The turbulent viscosity coefficient is calculated using the k-ε model:

$$\mu_t=\frac{f_\mu C_\mu \rho k^2}{\varepsilon} \tag{5}$$

To ensure the accuracy of numerical calculations in the wall region, a low Reynolds number k-ε model is adopted. To avoid the use of wall functions, the low Reynolds number k-ε model proposed by Jones and Launder (1973) is applied to describe the flow near the pipe wall. This model enhances the precision of capturing the turbulent characteristics in the vicinity of the wall, where the effects of viscosity and turbulence are significant.

Turbulent pulsation kinetic energy k equation:

$$\frac{1}{l_\eta l_\xi}\frac{\partial}{\partial \xi}\left(\Gamma_k\frac{\partial k}{\partial \xi}\right)+\frac{1}{l_\eta l_\xi}\frac{\partial}{\partial \eta}\left(\Gamma_k\frac{\partial k}{\partial \eta}\right)=\rho\varepsilon-\frac{1}{l_\eta l_\xi}\mu_t\left[\left(\frac{\partial u}{\partial \eta}\right)^2+\left(\frac{\partial u}{\partial \xi}\right)^2\right] \tag{6}$$

Turbulent dissipation rate ε equation:

$$\frac{1}{l_\eta l_\xi}\frac{\partial}{\partial \xi}\left(\Gamma_e\frac{\partial \varepsilon}{\partial \xi}\right)+\frac{1}{l_\eta l_\xi}\frac{\partial}{\partial \eta}\left(\Gamma_e\frac{\partial \varepsilon}{\partial \eta}\right)=C_2 f_2\rho\frac{\varepsilon^2}{k}-\frac{1}{l_\eta l_\xi}C_1 f_1\frac{\varepsilon}{k}\mu_t\left[\left(\frac{\partial u}{\partial \eta}\right)^2+\left(\frac{\partial u}{\partial \xi}\right)^2\right] \tag{7}$$

where $\Gamma_k = \mu_m + \mu_t/\sigma_k, \Gamma_\varepsilon = \mu_m + \mu_t/\sigma_\varepsilon$.

When the k-ε model is used to solve the turbulent flow problem, the governing equations include the momentum Eq. (2), k Eq. (6), ε Eqs. (7) and (5). Two constants (σ_k, σ_ε) and three coefficients (C_1, C_2, C_μ) are introduced in the system of equations. According to the turbulence model proposed by Lam-Bremhorst, the values of these five empirical constants are: $\sigma_k = 1$, $\sigma_\varepsilon = 1.3$, $C_\mu = 0.09$, $C_1 = 1.92$, $C_2 = 1.3$.

In order to close the k-ε model, the Lam and Bremhorst (1981) is used to calculate the decay function of turbulent pulsations due to wall effects f_μ, f_1 and f_2:

$$f_\mu=[1-\exp(-0.0165\mathrm{Re}_k)]^2\left(1+\frac{\zeta}{\mathrm{Re}_t}\right) \tag{8}$$

$$f_1=1+\left(\frac{0.05}{f_\mu}\right)^3 \tag{9}$$

$$f_2=1-\exp\left(-\mathrm{Re}_t^2\right) \tag{10}$$

where $\mathrm{Re}_k = \rho\sqrt{k}\,d_k/\mu_m$, $\mathrm{Re}_t = \rho k^2/(\mu_m\varepsilon)$; d_k is the normal distance to the interface. In oil-water stratified flow, both the pipe wall and oil-water interface generate wall effects that suppress turbulence development. Thus, the wall distance d_k used in turbulence modeling should be the smaller value between the distance from the pipe wall and the distance from the oil-water phase interface:

$$d_k = \min(d_W, d_l) \tag{11}$$

where d_W denotes the distance from the computational point to the pipe wall, m, and d_l represents the distance to the oil-water interface, m. Newton and Masud (2000, 2001) corrected the equation for ζ in two-phase flow:

$$\zeta = 20.5\left[1 - 1.45\exp\left(-1.4\times10^{-4}\mathrm{Re}\right)\right] \tag{12}$$

2.4. Boundary conditions

Based on the flow and heat transfer characteristics of oil and water phases in oil-water two-phase stratified flow, the computational domain boundaries are defined as: the pipe wall boundary, the oil-water interface boundary, and the vertical centerline boundary of the pipe.

2.4.1. Flow calculation boundary

(1) Pipe wall boundary $\xi = \theta_0, \xi = \theta_0 + \pi$

The no-slip solid-wall boundary condition is applied to the pipe wall. This means that at the pipe wall, the flow velocity, turbulent kinetic energy, and turbulent viscosity coefficient for both phases are zero. The specific boundary conditions are as follows:

$$u_W = 0, k_W = 0, \mu_{t,W} = 0 \tag{13}$$

Since the turbulent viscosity coefficient of the fluid at the wall $\mu_{t,W} = 0$, the effective viscosity coefficient of the fluid at the wall μ_e is equal to the molecular viscosity coefficient, i.e., $\mu_e = \mu_m$. The boundary condition of the turbulent dissipation ε at the wall is as follow:

$$\varepsilon_W = \frac{\mu_m}{\rho}\left(\frac{\partial^2 k}{\partial \xi^2}\right)_W \tag{14}$$

Eq. (14) contains the turbulent kinetic energy term, which can be complex to apply directly. Therefore, Newton and Masud (2000, 2001) simplified the pipe wall boundary condition for turbulent dissipation as follows:

$$\left.\frac{\partial \varepsilon}{\partial \xi}\right|_W = 0 \tag{15}$$

(2) Oil-water phase interface boundary $\xi = \theta^*$

In contrast to the pipe wall boundary condition, the oil-water phase interface boundary condition involves the coupling of the oil and water phases of the flow. Newton and Masud (2000, 2001) demonstrated that the presence of a phase interface reduces the development of turbulence, and similar to a pipe wall, the phase interface can be treated as a moving wall. The boundary condition at the oil-water phase interface are as follow:

$$k_{l,O} = k_{l,W} = 0 \quad \left.\frac{\partial \varepsilon}{\partial \xi}\right|_l = 0 \quad (\mu_t)_{l,O} = (\mu_t)_{l,W} = 0 \tag{16}$$

At the oil-water phase interface, the velocities of the oil and water phases are continuous, and the shear stresses are equal. The boundary conditions at the oil-water phase interface is as follows:

$$u_{l,O} = u_{l,W} \tag{17}$$

To accurately account for the interactions between the oil and water phases in stratified flow, the momentum transfer control equations for the oil and water phases are solved separately. Initially, the velocity field of the oil phase is obtained. The velocity of the oil phase at the oil-water interface is then used as the boundary condition for solving the water phase. However, this approach only considers the influence of the oil-phase flow on the water-phase flow, and neglects the reciprocal influence of the water phase on the oil phase. To address this limitation, the equal shear stress boundary condition the oil-water interface is introduced for both the oil and water phases. This ensures that the interaction between the two phases is accurately captured. The boundary conditions at the oil-water interface are therefore:

$$\tau_{l,O} = \tau_{l,W} \tag{18}$$

(3) Pipe vertical center boundary $\eta = 0$

Since the flow regions of the oil and water phases are symmetric about the vertical centerline (NQ) of the pipe, several properties exhibit specific behaviors at this central axis:

$$\frac{\partial u}{\partial \eta} = 0, \frac{\partial k}{\partial \eta} = 0, \frac{\partial \varepsilon}{\partial \eta} = 0 \tag{19}$$

2.4.2. Heat transfer calculation boundary

In the context of modeling oil-water two-phase stratified flow, the boundaries of the computational domain are crucial for accurately simulating the flow dynamics and heat transfer. Below is a concise description of each boundary.

(1) Pipeline inlet boundary $x = 0$

For the oil-water two-phase stratified flow with fully developed flow and heat transfer, a uniform temperature distribution in the cross-section at the pipe inlet is specified as T_b, the inlet ($x = 0$) temperature for both liquid phases.

$$T = T_b \tag{20}$$

(2) The upper wall boundary $\xi = \theta_0$

The upper wall boundary refers to the portion of the pipe wall contacting the oil phase, with constant heat flow boundary conditions applied at the upper wall:

$$h_e(T_{wall} - T_{envir}) = \lambda_O \frac{\partial T}{l_{\xi}\partial \xi} \tag{21}$$

The heat transfer coefficient h_e of the pipe to the environment takes into account the thermal resistance of the pipe wall, the insulation, and the outer wall of the pipe to heat transfer to the environment.

$$\frac{1}{h_e D_{in,in}} = \frac{1}{2\lambda_{pipe}}\ln\frac{D_{in,out}}{D_{in,in}} + \frac{1}{2\lambda_{ins}}\ln\frac{D_{out}}{D_{in,in}} + \frac{1}{h_o D_{out}} \tag{22}$$

where, h_e pipeline external effective heat transfer coefficient, W/(m^2·K); $D_{in,in}$, $D_{in,out}$, D_{out}, respectively, for the inner diameter of the pipeline, pipeline outer diameter, the outer diameter of the insulation layer, m; λ_{pipe}, λ_{ins}, respectively, for the pipeline and the insulation layer of the coefficient of thermal conductivity, W/(m·K); h_o for the pipeline outside the surface of the exothermic coefficient of the surrounding medium, W/(m^2·K).

(3) Oil-water phase interface boundary $\xi = \theta^*$

In contrast to the pipe wall boundary condition, the oil-water phase interface boundary condition involves heat transfer between the oil and water phases, where the temperatures of the oil and water phases are equal at the oil-water interface.

$$T_{\mathrm{int,O}} = T_{\mathrm{int,W}} \tag{23}$$

To address the influence of both phases on heat transfer at the oil-water interface in stratified flow, a boundary condition of equal heat flux between the oil and water phases at the interface is introduced. This ensures that the heat flux from the interface to the oil phase is equal to the heat flux from the interface to the water phase, thereby accounting for mutual heat exchange between the phases. Consequently, this condition ensures that the temperature boundary conditions used for solving the water phase appropriately incorporate the combined influence of the heat transfer associated with the oil phase and the heat transfer associated with the water phase at the interface, thus accurately capturing the mutual thermal interaction between the two phases.

$$q_{\mathrm{int,O}} = q_{\mathrm{int,W}} \tag{24}$$

(4) Boundary of the lower wall surface of the pipe wall $\xi = \theta_0 + \pi$

The constant heat flow boundary conditions at the lower wall refer to maintaining a steady heat flux applied to the surface. This condition ensures a constant heat flow between the pipe wall from and the environment. Mathematically, this is expressed as:

$$h_{\mathrm{e}}(T_{\mathrm{wall}} - T_{\mathrm{envir}}) = \lambda_{\mathrm{W}} \frac{\partial T}{l_{\xi} \partial \xi} \tag{25}$$

(5) Pipe vertical center boundary $\eta = 0$

In the context of symmetric flow and heat transfer regions about the vertical centerline of the pipe, the temperature gradient for both the oil and water phases is zero at the vertical center. This symmetry implies that at the midpoint of the pipe:

$$\frac{\partial T}{\partial \eta} = 0 \tag{26}$$

A core assumption of this model is the existence of a sharp, non-mass-transferring geometric interface between the oil and water phases. This assumption is reasonable for low-shear, stable stratified flow. However, at high flow rates or in inclined pipes, the interface may become mixed, emulsified, or wavy, potentially reducing the model's predictive accuracy. Accounting for the thermal resistance and mass transfer effects of an interfacial mixing layer is an important direction for future model improvement.

2.5. The continuity equation

The continuity equation for immiscible oil-water two-phase flow ensures that the mass flow rates of both phases remain constant at any cross-section along the pipe flow direction. This equation is typically expressed as:

$$G_{\mathrm{in,W}} = \int_{A_{\mathrm{W}}} \rho_{\mathrm{W}} u_{\mathrm{W}} \mathrm{d}A \tag{27}$$

$$G_{\mathrm{in,O}} = \int_{A_{\mathrm{O}}} \rho_{\mathrm{O}} u_{\mathrm{O}} \mathrm{d}A \tag{28}$$

where, $G_{\mathrm{in,O}}$ and $G_{\mathrm{in,W}}$ are the mass flow rates of the oil and water phases, kg/s, respectively; ρ_{O} and ρ_{W} are the densities of the oil and water phases, kg/s, respectively; u_{O} and u_{W} are the axial flow rates of the oil and water phases, m/s, respectively; A_{O} and A_{W} are the circulation areas of the oil and water phases, m^2, respectively.

2.6. Numerical calculation methods

2.6.1. Generalized governing equations

By comparing the momentum transfer Eq. (2), the energy transfer Eq. (3), the turbulence pulsation kinetic energy Eq. (6), and the turbulence dissipation rate Eq. (7), it can be found that the governing equation can be expressed in the following unified form:

$$\frac{1}{l_{\eta} l_{\xi}} \frac{\partial}{\partial \xi}\left(\Gamma_{\phi} \frac{\partial \phi}{\partial \xi}\right) + \frac{1}{l_{\eta} l_{\xi}} \frac{\partial}{\partial \eta}\left(\Gamma_{\phi} \frac{\partial \phi}{\partial \eta}\right) = u \frac{\partial \phi}{\partial x} + S_{\phi} \tag{29}$$

where ϕ is the generalized variable; Γ_{ϕ} and S_{ϕ} are the generalized diffusion coefficient and the generalized source term, respectively.

The generalized diffusion coefficients and source terms for the variables velocity, temperature, turbulent kinetic energy k, and turbulent dissipation rate ε are listed in Table 1. The governing equations for these variables share a consistent generalized form, facilitating uniform discretization and solution methods. The only differences among the generalized governing equations for each variable are in the diffusion coefficients, source terms, and boundary conditions.

2.6.2. Discretization of the governing equations

The governing equations for the oil and water phases under oil-water two-phase stratified flow conditions are formally identical, and their discretized equations exhibit the same form, differing only in the specific coefficients. For the generalized governing equations, the numerical solution is obtained using the finite difference method:

$$A_{\mathrm{P}}\phi_{i,j,k} + A_{\mathrm{N}}\phi_{i+1,j,k} + A_{\mathrm{S}}\phi_{i-1,j,k} + A_{\mathrm{W}}\phi_{i,j+1,k} + A_{\mathrm{E}}\phi_{i,j-1,k} = A_{\mathrm{B}}\phi_{i,j,k-1} + S_{\phi}\left(l_{\eta} l_{\xi}\right)_{i,j} \tag{30}$$

where the expressions for the A_{N}, A_{S}, A_{W}, and A_{E} coefficients are similar.

$$A_{\mathrm{N}} = -\frac{2}{\Delta\xi_{i+1,j,k} + \Delta\xi_{i,j,k}} \frac{\left(\Gamma_{\phi}\right)_{i+1,j,k} + \left(\Gamma_{\phi}\right)_{i,j,k}}{2} \frac{1}{\Delta\xi_{i+1,j,k}} \tag{31}$$

$$A_{\mathrm{B}} = \frac{u_{i,j,k}}{\Delta z_{i,j,k}} \left(l_{\eta} l_{\xi}\right)_{i,j} \tag{32}$$

$$A_{\mathrm{P}}\phi_{i,j,k} = A_{\mathrm{N}} + A_{S} + A_{\mathrm{W}} + A_{\mathrm{E}} \tag{33}$$

Table 1
Generalized governing equations in bipolar coordinate system.

ϕ	Γ_{ϕ}	S_{ϕ}	$u\frac{\partial \phi}{\partial x}$
u	$\mu_{\mathrm{m}} + \mu_{\mathrm{t}}$	$\frac{\mathrm{d}P}{\mathrm{d}x}$	0
T	$\frac{\mu_m}{\mathrm{Pr}} + \frac{\mu_t}{\mathrm{Pr}_T}$	0	$u\frac{\partial T}{\partial x}$
k	$\mu_{\mathrm{m}} + \frac{\mu_{\mathrm{t}}}{\sigma_k}$	$\varepsilon\rho - \frac{1}{l_{\eta} l_{\xi}} \mu_t \left[\left(\frac{\partial u}{\partial \eta}\right)^2 + \left(\frac{\partial u}{\partial \xi}\right)^2\right]$	0
ε	$\mu_{\mathrm{m}} + \frac{\mu_{\mathrm{t}}}{\sigma_{\varepsilon}}$	$c_2 f_2 \rho \frac{\varepsilon^2}{k} - \frac{1}{l_{\eta} l_{\xi}} c_1 f_1 \mu_{\mathrm{t}} \frac{\varepsilon}{k} \left[\left(\frac{\partial u}{\partial \eta}\right)^2 + \left(\frac{\partial u}{\partial \xi}\right)^2\right]$	0

2.6.3. Calculation process

The governing equations are discretized using the finite difference method and solved with the Gauss-Seidel iteration. This approach couples the flow and heat transfer control equations to determine the oil-water temperature distribution of the oil and water phases in the pipeline. The solution process for oil-water two-phase stratified flow involves the following main steps, illustrated in Fig. 3.

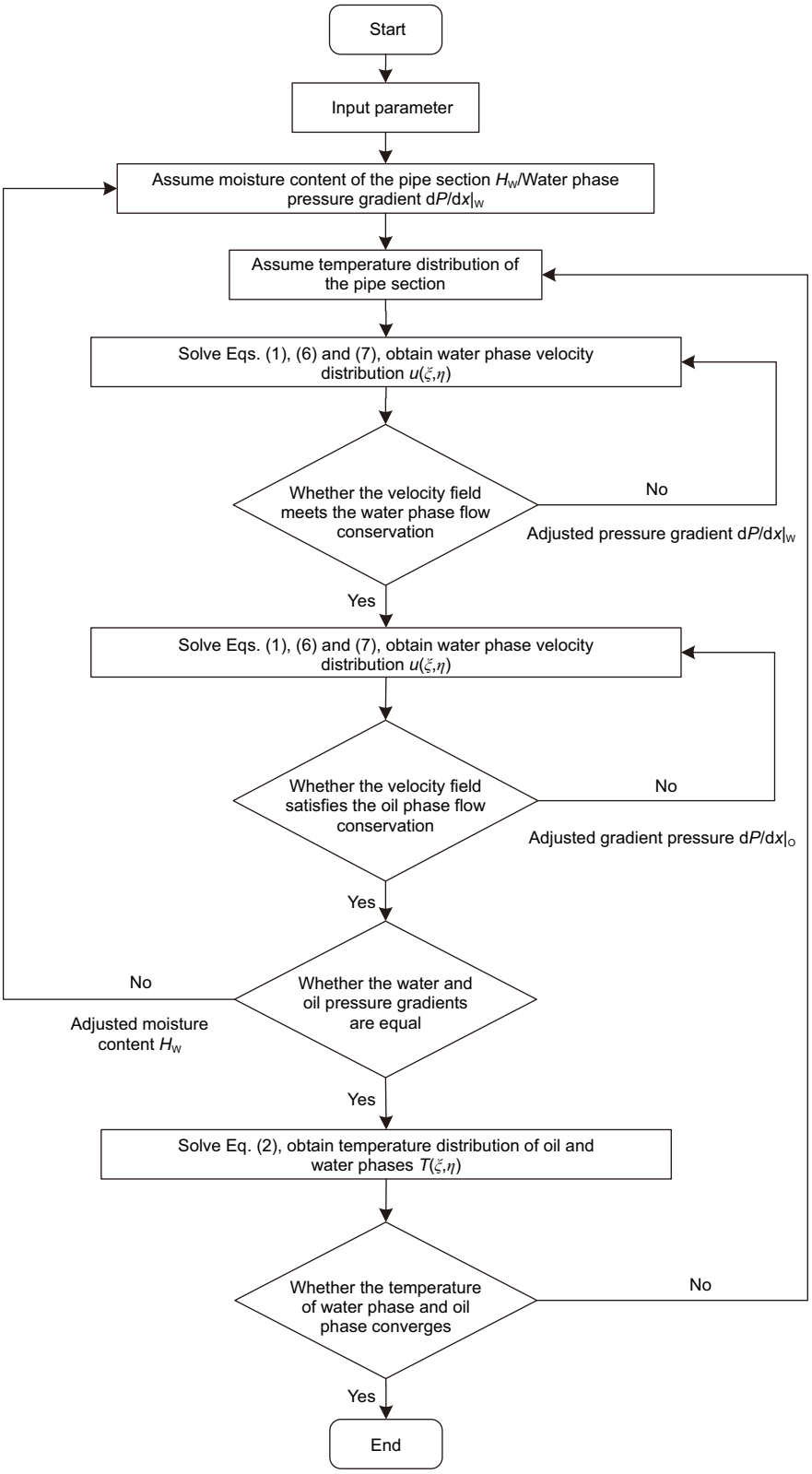

Fig. 3. Numerical calculation flow of oil-water two-phase stratified flow and heat transfer.

1) Perform hydraulic calculations using a one-dimensional two-fluid model (Liu et al., 2008), and preliminarily estimate the temperature of the oil and water phases at each calculation node using a one-dimensional thermal calculation model for oil-water stratified flow (Liu et al., 2008).
2) Calculate the temperature of the oil and water phases at each calculation node and determine the temperature-dependent property parameters.
3) Calculate the flow characteristics of the oil and water phases.
4) Solve the oil-phase and water-phase energy transfer equations using the finite difference until convergence.

3. Validation of models

To verify the accuracy of the heat transfer calculation model for oil-water two-phase stratified flow, experiments were performed on a oil-water two-phase flow heat transfer loop. It should be noted that the model validation in this work, conducted on a laboratory-scale oil-water two-phase flow loop, is primarily based on the integral quantity of the outlet average temperature. The current experimental setup could not provide measurement data for the internal three-dimensional temperature field, phase interface shape, or local heat flux density. As such, the accuracy of the model in resolving these fine-grained, three-dimensional details is a critical aspect that awaits further verification using more sophisticated measurement methods in subsequent studies.

3.1. Experimental device for heat transfer characteristics

The oil-water two-phase flow heat transfer experimental loop consists of seven main components: the oil supply system, water supply system, gas supply system, piping system, separation system, temperature control system, and data measurement and signal acquisition system, as shown in Fig. 4. The length of the 304 stainless steel pipeline system is 30 m and the inner diameter is 25.4 mm. A water bath controller regulates the jacket temperature, enabling heat transfer experiments under single-phase oil and two-phase flow conditions.

Oil and water flow from separate tanks through dedicated pumps and pipelines, merging via a Y-mixer into the main pipe. After passing through the fully developed flow and heat transfer section, they enter the test section. In this section, the oil and water flow temperatures and the lower pipe wall temperature are measured to study heat transfer. The oil and water then flow into an oil-water separator and return to their respective tanks, completing the cycle. The independent containers and piping systems for oil and water prevent emulsion formation and allow easy adjustment of flow rate and temperature. Temperature controllers and heating equipment in the tanks regulate the oil and

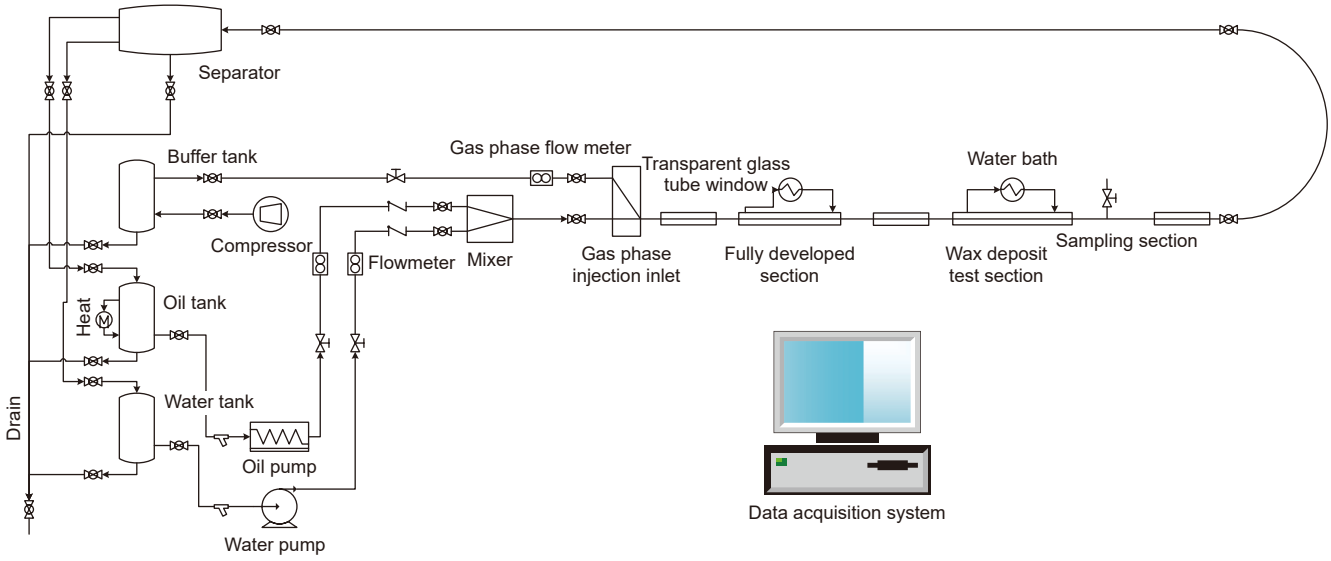

Fig. 4. Schematic diagram of the experimental loop of oil-water two-phase flow wax deposition.

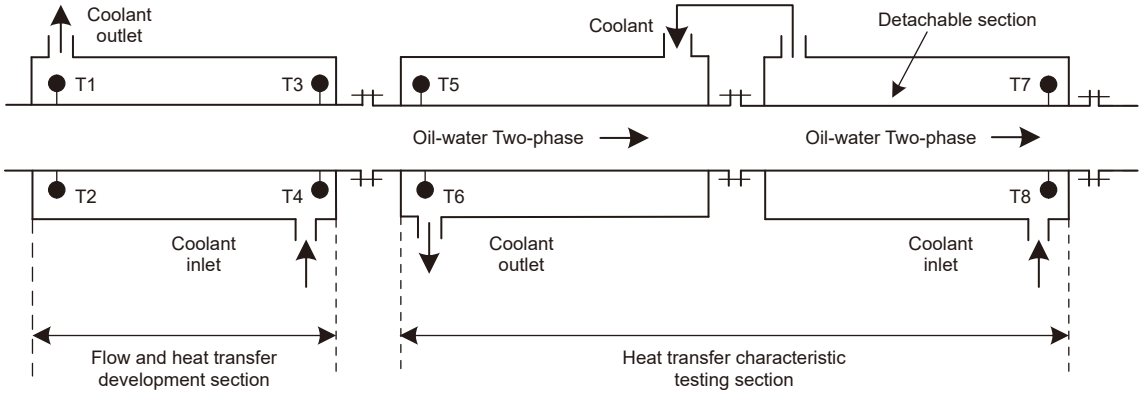

Fig. 5. Experimental section of oil-water two-phase flow heat transfer characteristic.

water temperatures. The test section features a pipe-in-pipe casing structure, with a cooling medium in the casing sandwich regulated by a thermostatic water bath controller.

The experimental section for characterizing heat transfer in oil-water two-phase stratified flow consists of two segments, as shown in Fig. 5. The first section is a 5-m-long casing-section that allows the oil-phase and water-phase fluids to reach a fully developed flow and heat transfer state. The second section, a 7-m-long test section, measures the heat transfer characteristics. The bottom and top temperature sensor, i.e. T5 and T6, measures entry temperature of water (T_{wi}) and oil phase (T_{oi}) respectively. The bottom and top temperature sensor, i.e. T7 and T8, measures exit temperature of water (T_{we}) and oil phase (T_{oe}) respectively. The TMR31 Pt100 resistance type temperature sensor is used to measure the temperature of the oil or water. It has a standard accuracy of $\pm$0.15 °C. The test section, with a DN25 inner pipe, is encased in a DN70 pipe, forming a casing. A thermostatic water bath circulates a cooling medium (glycol and water) through the casing to control the temperature. The flow direction of the cooling medium is opposite to that of the oil-water medium in the inner pipe. To minimize ambient temperature effects, the casing is insulated. The dimensions of the test pipe section for heat transfer characteristics are detailed in Table 2.

3.2. Experimental materials

The oil-water two-phase stratified flow heat transfer experiments require stable stratified flow pattern in the annular channel. To improve the efficiency of oil-water separation, EXXSOL D80 solvent oil, produced by ExxonMobil Chemical Services (Shanghai) Co., Ltd., and deionized water are used as the experimental mediums. D80 solvent oil is a de-aromatized, desulfurized solvent with a carbon number mainly between C12 and C15. It is a colorless, transparent, non-volatile liquid. The resistivity of deionized water is greater than 15 MΩ cm. The basic physical properties of the solvent oil and deionized water are shown in Table 3.

3.3. Experimental methods and procedures

The experimental process for the oil-water two-phase stratified flow heat transfer loop involves selecting stable flow conditions and measuring the temperature of the oil-water stratified flow. The main steps are as follows.

1) Adjust the circulating water tank temperature to heat the solvent oil to the required experimental temperature and set the hot water tank to heat the water phase.
2) Maintain the heated solvent oil and water for 3 h to ensure uniform temperatures and experiment repeatability.
3) Transfer a specified amount of solvent oil and water to the oil-water separator, and activate the separator heating device and temperature controller.
4) Set the circulating coolant temperature of the thermostatic water bath in the test section and all other baths throughout the piping system to the required experimental temperature.
5) Once the fluid medium in the oil tank, water tank, and separator has reached and stabilized at the designated experimental temperature, initiate the operation of the oil and water transfer pumps. Adjust their speeds to achieve the desired flow rates, and activate the data acquisition system to record temperatures at both the inlet and outlet of the test section. When these temperatures have stabilized, maintain consistent experimental conditions for a duration of 10 min.
6) Adjust the pump speeds as needed for subsequent experiments conditions.

3.4. Experimental scheme and results

The temperature controller was calibrated to maintain the oil-phase and water-phase tubular flow medium at 35 °C, while the cooling medium in the heat transfer characteristics experimental section was maintained at 20 °C. A frequency converter was employed to adjust the pump speed, thereby regulatingthe flow rates of both the oil and water phases. The apparent flow rate of the oil phase varied from 0.1 m/s to 0.4 m/s, with inlet water content ranging from 20% to 80%. A transparent glass observation window confirmed that the oil-water two-phase flow within the pipeline exhibited stratified flow by the mega speed camera, with the oil phase consistently occupying the upper portion of the pipeline and the water phase residing in the lower portion as shown in Fig. 6.

Table 2
Dimensions of experimental section of oil-water two-phase flow heat transfer characteristics.

Internal diameter, mm	Pipe wall thickness, mm	Length of pipeline development section, m	Length of pipe test section, m
25.4	2.5	5	7

Table 3
Physical properties of experimental materials.

	Density, kg/m^3	Thermal conductivity, W/(m·K)	Thermal diffusion coefficient, m^2/s	Specific heat capacity, J/(kg·K)
Solvent oil	795.0	0.17	0.12×10^{-6}	1890
Deionized water	999.3	0.59	0.14×10^{-6}	4190

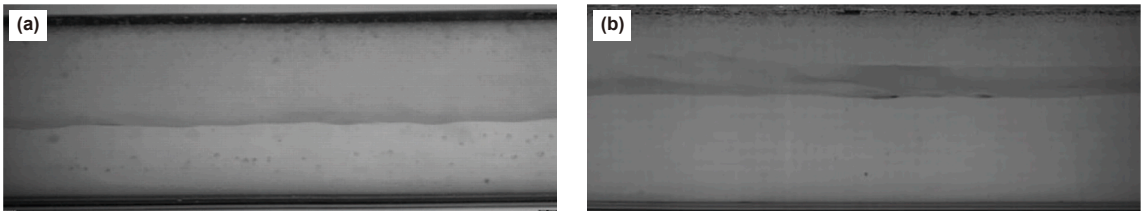

Fig. 6. Photographs of stratified flow. **(a)** Water content 20%. **(b)** Water content 70%.

Table 4
Experimental scheme of oil-water two-phase stratified flow heat transfer characteristics of the flow loop.

Serial number	Oil phase flow rate, m/s	Water phase flow rate, m/s	Inlet water content
1	0.5	0	0
2	0.4	0.1	20%
3	0.35	0.15	30%
4	0.3	0.2	40%
5	0.25	0.25	50%
6	0.15	0.35	70%
7	0.1	0.4	80%
8	0	0.5	100%

Table 5
Experimental results of oil-water two-phase stratified flow heat transfer characteristics of the flow loop.

Serial number	Oil phase flow rate, m/s	Water phase flow rate, m/s	Inlet water content	Inlet temperature, °C		Outlet temperature, °C	
				Oil phase	Water phase	Oil phase	Water phase
1	0.5	0	0	34.9	–	33.9	–
2	0.4	0.1	20%	34.8	34.8	33.5	33.2
3	0.35	0.15	30%	34.9	35	33.4	32.9
4	0.3	0.2	40%	34.8	34.9	33.2	32.7
5	0.25	0.25	50%	35	34.9	33.1	32.6
6	0.15	0.35	70%	34.9	34.9	32.9	32.1
7	0.1	0.4	80%	34.9	35	32.2	31.8
8	0	0.5	100%	–	34.8	–	31.5

To achieve a more comprehensive understanding of the heat transfer characteristics in oil-water two-phase stratified flow, experiments were also conducted under single-phase conditions for both oil and water. The experimental scheme for the heat transfer loop is detailed in Table 4. Temperature sensors installed at the upper and lower sections of both the inlet and outlet of the heat transfer characteristic test section recorded the temperatures of the oil-water two-phase flow, as presented in Table 5.

3.5. Comparison of simulation results

During the oil-water two-phase stratified non-isothermal flow, the pipe cross-section average temperatures $T_{b,O}$ and $T_{b,W}$ of the oil and water phases are calculated using velocity as a weighting factor (Li et al., 2018):

$$T_{b,O}=\frac{\int_{A_O} T(\xi,\eta)u_O(\xi,\eta)\mathrm{d}A}{\int_{A_O} u_O(\xi,\eta)\mathrm{d}A} \tag{34}$$

$$T_{b,W}=\frac{\int_{A_W} T(\xi,\eta)u_W(\xi,\eta)\mathrm{d}A}{\int_{A_W} u_W(\xi,\eta)\mathrm{d}A} \tag{35}$$

where $T(\xi, \eta)$ is the temperature distribution of the oil and water phases in the pipe cross-section, °C; $u_O(\xi, \eta)$ and $u_W(\xi, \eta)$ are the axial flow rates of the oil and water phases, m/s, respectively; A_O and A_W are the circulation areas of the oil and water phases, m^2, respectively.

The temperature drop ΔT_b of the oil or water phase is:

$$\Delta T_b = T_{b,inlet} - T_{b,outlet} \tag{36}$$

where $T_{b,inlet}$ is the temperature of the oil or water phase at the inlet of the pipe, °C; $T_{b,outlet}$ is the temperature of the oil or water phase at the outlet of the pipe, °C.

The relative error T_{RE} of the model predicted value is:

$$T_{RE}=\frac{\Delta T_{b,predicted}-\Delta T_{b,measured}}{\Delta T_{b,measured}} \tag{37}$$

where $\Delta T_{b,predicted}$ is the calculated value of temperature drop in the oil or water phase, °C; $\Delta T_{b,measured}$ is the experimental value of temperature drop in the oil or water phase, °C.

The convective heat transfer coefficient of the cooling medium flowing in the casing against the outer wall of the tube in the test section is calculated using Eq. (38).

$$h_{clnt}=\frac{Nu_{clnt}\lambda_{clnt}}{D_{hy,clnt}} \tag{38}$$

where, h_{clnt} is the convective heat transfer coefficient of the cooling medium, W/(m^2·K); λ_{clnt} is the thermal conductivity of the cooling medium, W/(m·K); $D_{hy,clnt}$ is the equivalent pipe diameter of the cooling medium flow, m; Nu_{clnt} is the coolant Nusselt number.

Nu_{clnt} is obtained according to the Gnielinski model (Gnielinski, 2009):

$$Nu_{clnt}=\frac{\left(\frac{f}{8}\right)Re_{clnt}\,Pr_{clnt}}{k_1+12.7\sqrt{\frac{f}{8}}\left(Pr_{clnt}^{\frac{2}{3}}-1\right)}x_1k_2k_3 \tag{39}$$

where

$$f=\left(1.8\log Re^{*}_{clnt}-1.5\right)^{0.5} \tag{40}$$

$$x_1=\left(1+\frac{D_{hy,clnt}}{L_{tot}}\right)^{\frac{2}{3}} \tag{41}$$

$$k_1=1.07+\frac{900}{Re_{clnt}}-\frac{0.63}{1+10\,Pr_{clnt}} \tag{42}$$

Table 6
Comparison of calculated and experimental values of oil-water two-phase average temperature.

Serial number	Oil phase flow rate, m/s	Water phase flow rate, m/s	Inlet water content	Oil phase outlet temperature, °C			Water phase outlet temperature, °C		
				Experimental value	Calculated value	Relative error, %	Experimental value	Calculated value	Relative error, %
1	0.5	0	0	33.9	34.58	2.01	–	–	–
2	0.4	0.1	20%	33.5	34.36	2.57	33.2	34.21	3.04
3	0.35	0.15	30%	33.4	34.12	2.16	32.9	34.01	3.37
4	0.3	0.2	40%	33.2	33.95	2.26	32.7	33.58	2.69
5	0.25	0.25	50%	33.1	33.52	1.27	32.6	32.92	0.98
6	0.15	0.35	70%	32.9	31.82	−3.28	32.1	31.21	−2.77
7	0.1	0.4	80%	32.2	31.02	−3.66	31.8	30.28	−4.78
8	0	0.5	100%	–	–	–	31.5	30.57	−2.95

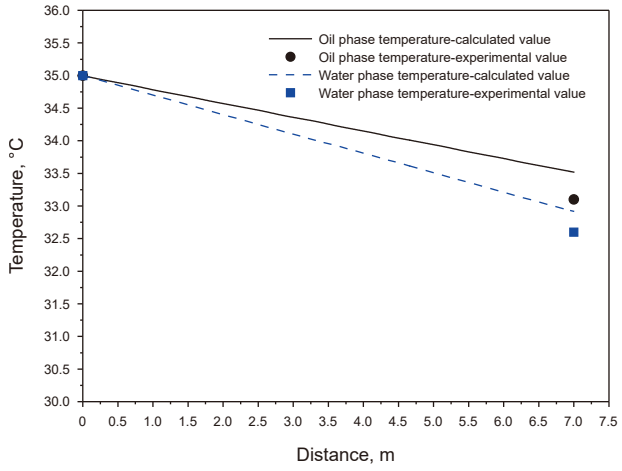

Fig. 7. Comparison of calculated temperature of oil-water two-phase stratified flow with experimental data.

$$k_2 = 0.75\psi^{-0.17} \tag{43}$$

$$k_3 = \left(\frac{\mathrm{Pr}_{\mathrm{clnt,Bulk}}}{\mathrm{Pr}_{\mathrm{clnt,Cold\ Wall}}}\right)^{0.11} \tag{44}$$

$$\psi = \frac{D_{\mathrm{in,out}}}{D_{\mathrm{out,in}}} \tag{45}$$

$$\mathrm{Re}^{*}_{\mathrm{clnt}} = \mathrm{Re}_{\mathrm{clnt}} \frac{(1+\psi^2)\ln\psi + (1-\psi^2)}{(1-\psi)^2 \ln\psi} \tag{46}$$

where $D_{\mathrm{out,in}}$ and $D_{\mathrm{in,out}}$ are the inner diameter of the casing and the outer diameter of the inner tube, m, respectively; $\mathrm{Re}_{\mathrm{clnt}}$ and $\mathrm{Pr}_{\mathrm{clnt}}$ are the coolant Reynolds number and Prandtl number, respectively; L_{tct} is the total length of the test section, m; λ_{clnt} is the thermal conductivity of the cooling medium, W/(m·K); μ_{clnt} is the dynamic viscosity of the cooling medium, Pa·s; C_{clnt} is the specific heat of the cooling medium, J/(kg·K); ρ_{clnt} is the density of the cooling medium, kg/m^3.

Table 6 compares the calculated and experimental values of the average temperatures of the oil and water phases at the exit of the test section under fully developed oil-water two-phase stratified flow conditions. The comparison is made for an oil-phase apparent flow rate ranging from 0.1 m/s to 0.4 m/s, inlet water content between 20% and 80%, and a combined oil-water flow rate of 0.5 m/s. The results show that the model accurately predicts the average temperatures of both phases, with an absolute relative error within 5% (including single-phase oil and water flow cases). The table also indicates that the oil phase's temperature is slightly higher than the water phase, though the difference is small. For single-phase oil flow heat transfer calculations, the physical properties and flow rate of the water phase are set to those of the oil phase, and vice versa for single-phase water flow heat transfer calculations.

The oil-water two-phase stratified flow heat transfer model was used to calculate the average temperature distribution of the oil and water phases along the pipeline in the test section, with an oil-phase flow rate of 0.25 m/s, a water-phase flow rate of 0.25 m/s, and an inlet water content of 50%, as shown in Fig. 7. The calculated outlet temperatures of the oil and water phases were compared with the measured values, showing a high accuracy with relative errors of 1.27% and 0.98%, respectively. Both calculated temperatures were slightly higher than the experimental values. The results indicate that under stratified flow conditions in the same pipe section, the oil phase temperature is always higher than the water phase temperature. The experimental measurements show a temperature difference of 0.5 °C at the test section exit, while the calculated value is 0.6 °C. As the fluid flows downstream, the temperature difference between the oil and water phases increases.

4. Calculation results and analysis

To further analyze the heat transfer characteristics of oil-water two-phase stratified flow, the calculation model was used to study the effect of inlet water content on the axial distribution of the average temperature of the oil and water phases. Additionally, the model was used to calculate the temperature distribution across the pipeline cross-section for both phases.

4.1. Pipe axial temperature distribution

In oil-water two-phase flow, the water content significantly affects the heat transfer process. To investigate this effect, the temperature distribution of two-phase flow with varying water content was simulated using a computational model. The simulation scenarios and conditions were aligned with experimental investigations on heat transfer characteristics of two-phase flow, as illustrated in Fig. 5 and Table 5, except the test section length in the simulation was 350 m.

Fig. 8 depicts the axial distribution of average temperatures for both oil and water phases at inlet water contents of 0%, 20%, 50%, 80%, and 100%. Due to variations in specific heat capacities and heat transfer coefficients, the temperature of the water phase consistently remains lower than that of the oil phase throughout the heat transfer process. Fig. 8(a) presents the simulation results for 0% (single-phase oil) and 100% (single-phase water) water

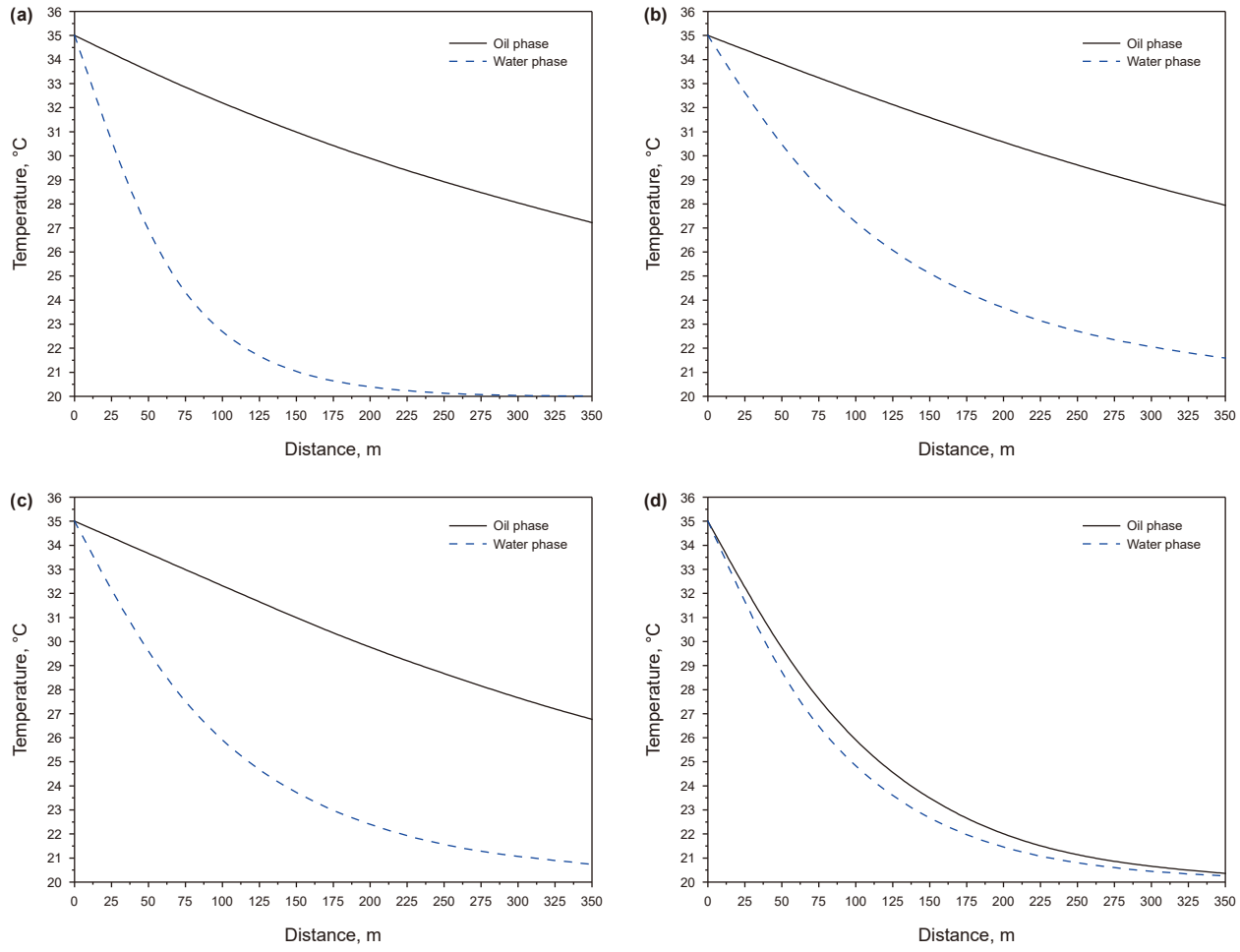

Fig. 8. Axial distribution of average temperatures of oil and water phases under different water content conditions. **(a)** Single-phase flow. **(b)** 20% water content. **(c)** 50% water content. **(d)** 80% water content.

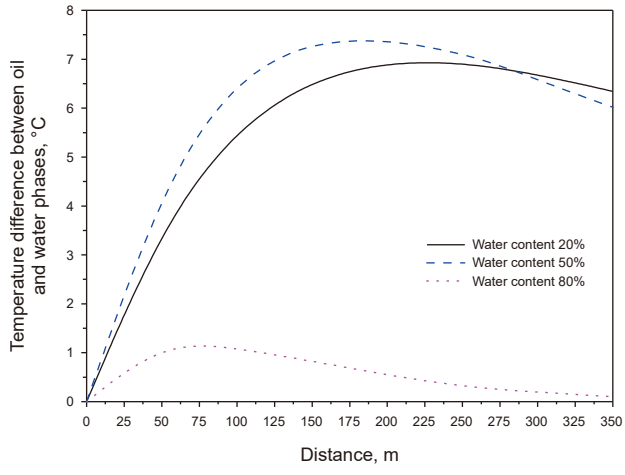

Fig. 9. Axial distribution of average temperature difference between oil and water phases under different water content conditions.

content. The water phase temperature decreases much faster than the oil phase due to the lower thermal resistance of water, leading to a faster heat transfer process compared to oil. The temperature distributions for water contents of 20%, 50%, and 80% are shown in Fig. 8(b) to 8(d). The temperature difference between the oil and water phases increases initially near the pipeline entrance and then gradually decreases downstream. Eventually, over a sufficiently long pipeline length, the temperatures of both phases approach ambient temperature, and the temperature difference diminishes to zero, as shown in Fig. 9.

As seen in Fig. 9, with increasing water content, the temperature difference between the oil and water phases initially increases, then decreases as the critical point approaches the pipe inlet. When the water content exceeds 80%, the temperature difference between the oil and water phases remains within 1 °C. In this scenario, the heat transfer approaches that of single-phase pipe flow and can be considered as quasi-single-phase heat transfer.

Due to the similar densities of the oil and water phases and assuming comparable volumetric flow rates, the mass flow rates are approximately the same. The water phase, having a higher specific heat capacity than the oil phase, carries more heat per unit mass. However, the thermal conductivity of the water phase is much higher than that of the oil phase. Consequently, under the same flow conditions, the temperature drop of the water phase is more significant than that of the oil phase, as shown in Fig. 8(c). The higher temperature of the oil phase causes continuous heat transfer from the oil to the water phase through the oil-water interface, increasing the water phase temperature and reducing the temperature difference between the phases.

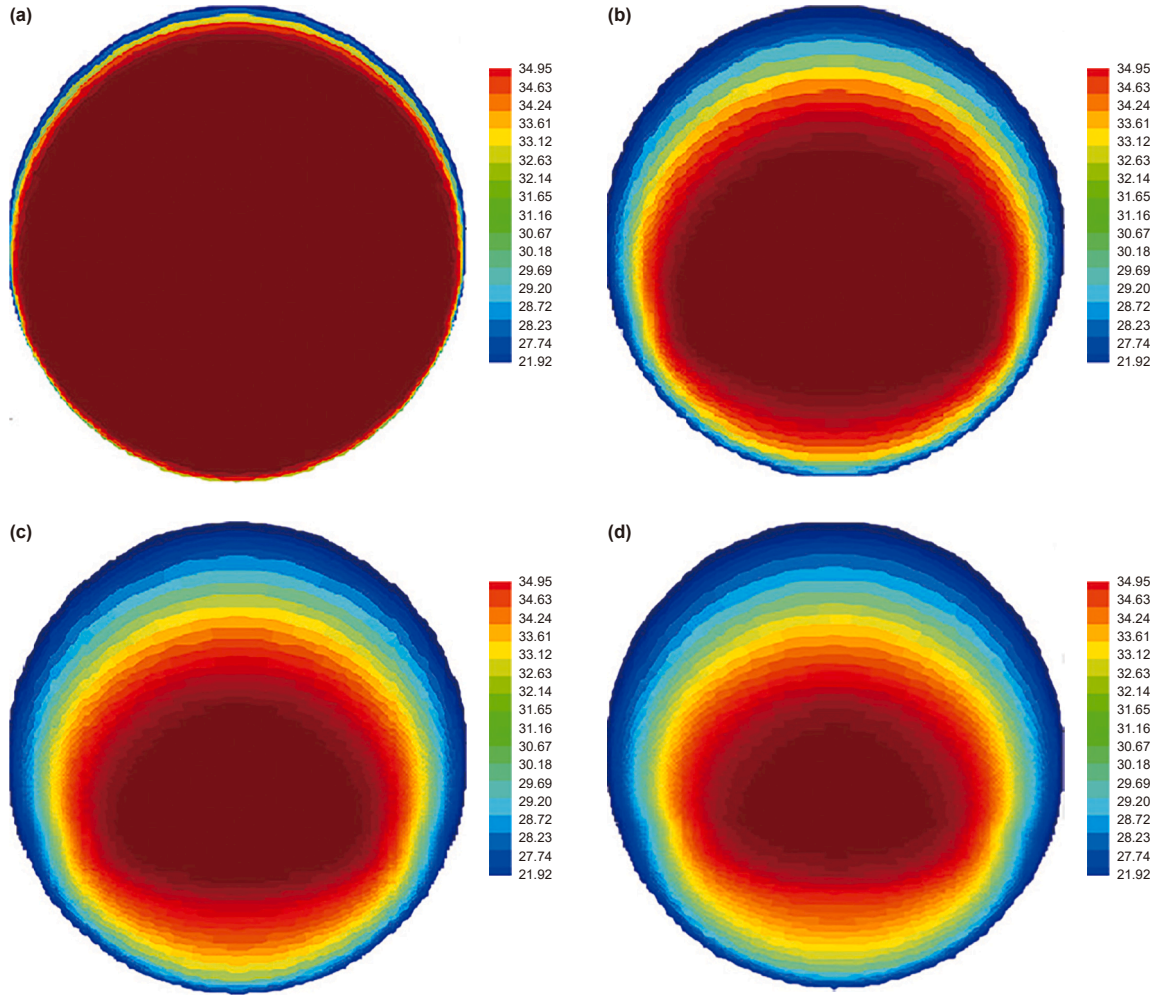

Fig. 10. Temperature distribution of pipe section at different axial positions. **(a)** 0.25 m. **(b)** 30 m. **(c)** 100 m. **(d)** 300 m.

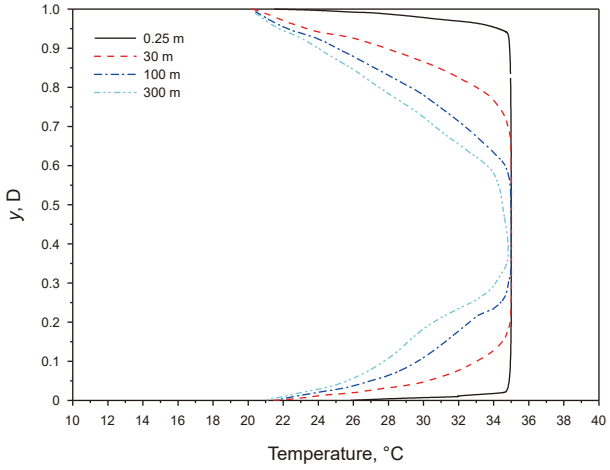

Fig. 11. Temperature distribution of the fluid cross-section on the centerline of the pipe at different axial positions.

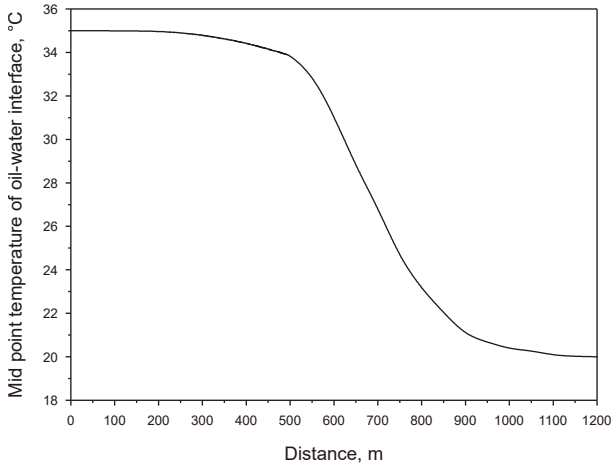

Fig. 12. Temperature distribution at the midpoint of the oil-water interface along the axial direction of the pipe.

4.2. Pipe cross-section temperature distribution

By using the oil-water two-phase stratified flow heat transfer model, under the conditions of an apparent flow velocity of 0.4 m/s for the oil phase, 0.1 m/s for the water phase, and a water content of 20%, the temperature distributions of the oil and water phases on the pipe sections at distances of 0.25, 30, 100, and 300 m from the inlet were obtained, as shown in Fig. 10. Additionally,

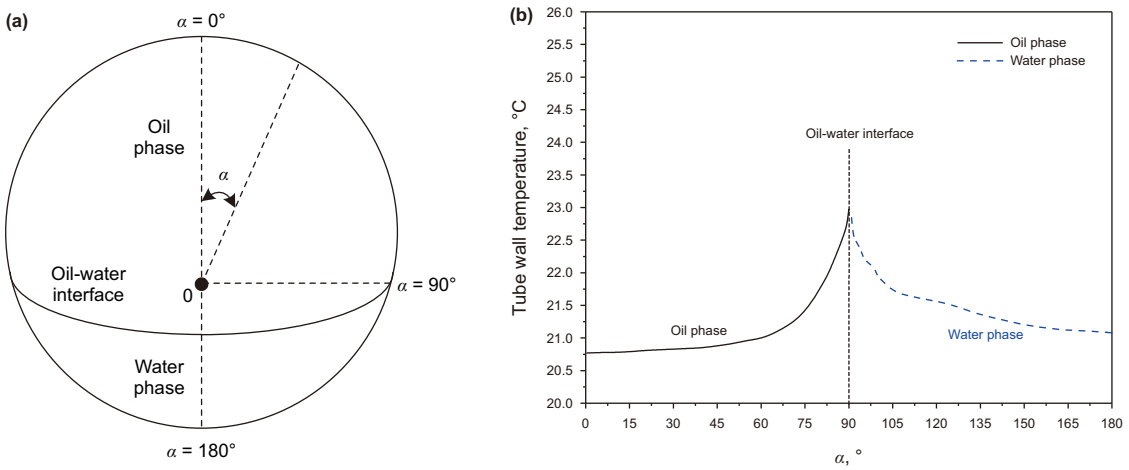

Fig. 13. Temperature distribution of the inner wall of the pipe. **(a)** Pipe cross-section. **(b)** Temperature distribution.

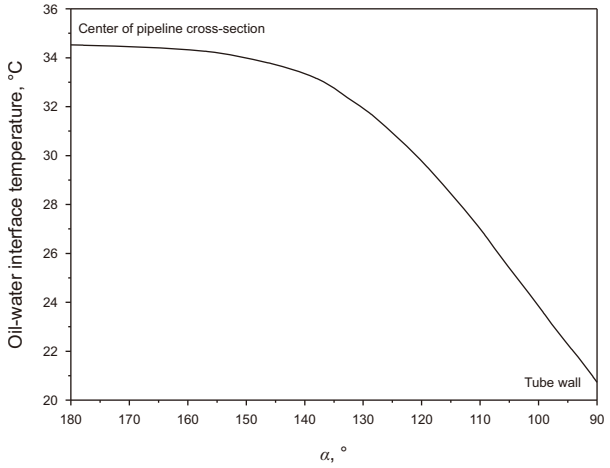

Fig. 14. Temperature distribution at the oil-water interface.

temperature distribution along the centerline of the pipeline cross-section is provided in Fig. 11.

From the temperature distribution observed in the pipeline cross-section, it can be noted that under the prevailing flow and heat transfer conditions, the temperature profiles of both the oil and water phases exhibit similarities to those found in single-phase flow, with relatively minor differences. The highest temperature within the liquid phase is located near the oil-water interface, surpassinge temperatures recorded at other positions within the oil and water phases. The temperatures for each phase decrease from the oil-water interface towards the pipeline wall. The oil-water interface functions as a dynamic conductive surface, facilitating heat transfer from the higher-temperature oil phase to the lower-temperature water phase. The temperature at the top of the pipe (oil-wetted wall) approximates the cooling medium temperature (20 °C), which is lower than that at the bottom (water-wetted wall).

The temperature distribution in the cross-section at different axial locations shows that the high-temperature region decreases along the pipeline due to the influence of the lower ambient temperature and convective heat transfer, leading to a decrease in temperatures of both the oil and water phases.

Fig. 12 presents the temperature distribution at the center point of the oil-water interface at different axial positions. Due to the small temperature difference between the oil-water interface and the surrounding liquid phase, the heat flux is minimal. A temperature decrease of only 1.05 °C is observed at the interface midpoint from pipe inlet to 300 m downstream. Relative stability in midpoint temperature is maintained within 150 m of the inlet. As the fluid flows further along the pipeline, the temperature drop increases, leading to a growing temperature gradient with increasing distance.

Comparing Figs. 8(b) and 12, it can be observed that the temperature change at the midpoint of the phase interface near the pipeline inlet shows a significant difference from the trend of the average temperature change of the oil and water phases in the pipeline cross-section. However, as the distance increases, the trend of change tends to be consistent.

Fig. 13 shows the temperature distribution on the inner wall of the pipe and at the oil-water phase interface in a cross-section located 100 m from the pipe inlet. Fig. 13(b) specifically details the temperature distribution of the inner wall infiltrated by the oil and water phases. An increase in inner wall temperature with angle α is recorded from the pipe top to the interface in the oil phase region. Conversely, a decrease with angle α is observed from the interface to the pipe bottom in the water phase region. The lowest temperature is located at the top of the pipe, while the highest temperature occurs at the oil-water phase interface.

The oil phase, with a lower specific heat capacity compared to the water phase, carries less heat near the pipe wall. Combined with lower thermal conductivity slower heat transfer rates are achieved. Consequently, the oil phase quickly loses heat at the inner wall and replenishes it slowly. In contrast, heat dissipation is delayed in the water phase with faster thermal recovery. Continuous interfacial heat transfer from oil to water phase reduces net heat loss in the water phase.

Fig. 14 illustrates the temperature distribution at the oil-water phase interface in a cross-section located 300 m from the pipeline inlet. A gradual temperature decrease from the centerline to the pipe wall is recorded. Moderate cooling is observed in the central region, while pronounced temperature reduction occurs near the pipe wall.

5. Conclusions

In this study, a heat transfer model for oil-water two-phase stratified flow was developed by coupling the momentum and

energy equations with the existing flow characteristics framework. Combined with appropriate boundary conditions, this model provides a numerical approach for coupled thermal-hydraulic analysis under stratified flow conditions. It quantitatively captures the effect of water content on the axial-averaged temperature distribution in both phases, as well as the axial, radial, and circumferential temperature evolution during non-isothermal flow. These findings offer fundamental insights for developing wax deposition models and clarifying their mechanisms in oil–water two-phase systems. The main conclusions are as follows.

(1) Due to differences in thermophysical properties, the oil phase exhibits a higher temperature than the water phase under laminar oil–water stratified flow conditions. The temperature difference between the two phases increases near the pipeline inlet and then gradually decreases along the flow direction until thermal equilibrium with the ambient environment is attained. As the water content rises, the interphase temperature difference transitions from an increasing to a decreasing trend, particularly in the inlet region. When the water content exceeds 80%, the temperature difference remains within 1 °C, and the overall heat transfer behavior approaches that of quasi-single-phase flow.
(2) The cross-sectional temperature distributions of both oil and water phases exhibit a pattern similar to that of single-phase flow, with the highest temperature observed near the oil–water interface. From the interface to the pipe wall, the temperature in both phases decreases monotonically. The interface acts as a conductive surface, facilitating heat transfer from the oil to the water phase. Along the inner wall, the temperature increases angularly from the top of the pipe to the interface and decreases from the interface to the bottom, resulting in the lowest temperature at the top and the highest at the interface.
(3) Along the axial direction, the temperature at the midpoint of the oil–water interface differs significantly from the cross-sectional average temperature near the inlet, but this discrepancy gradually diminishes downstream. As a result of convective heat transfer to the cooler ambient, high-temperature regions in the cross-section are progressively reduced, leading to a continuous decrease in the temperatures of both phases.
(4) A primary limitation of this study lies in the scope of model validation. The current model has been validated primarily against the integral quantity of the average outlet temperature at the laboratory scale. However, due to experimental constraints, localized details such as the internal three-dimensional temperature field, phase interface shape, and local heat flux density could not be measured and thus remain to be verified in the future using more advanced techniques. Furthermore, while the model demonstrates effectiveness at this scale, its applicability to actual industrial pipeline systems requires future systematic validation. This includes assessments across various pipe diameters (particularly large-diameter pipes), a wider range of flow rates, and different oil-water fluid properties to comprehensively evaluate the model's universality and robustness.

CRediT authorship contribution statement

Hui-Shu Liu: Writing – original draft, Resources, Funding acquisition, Formal analysis, Conceptualization. **Ji-Miao Duan:** Writing – review & editing, Writing – original draft, Resources, Funding acquisition, Data curation, Conceptualization. **Yong-Xiang Huang:** Visualization, Validation, Investigation. **Hao-Nan Li:** Writing – review & editing, Writing – original draft. **Shuo Xu:** Supervision, Methodology. **Shi-Ming Chen:** Supervision, Investigation. **Hui-Rong Huang:** Conceptualization.

Declaration of interests

The authors declare that they have no known competing financial interests or personal relationships that could have appeared to influence the work reported in this paper.

Acknowledgement

This research was funded by the National Natural Science Foundation of China (52302422, 52272338 and 52302402), the Natural Science Foundation of Chongqing, China (CSTB2024NSCQ-QCXMX0080 and CSTB2024NSCQ-MSX1039), and the Research Foundation of Chongqing University of Science and Technology (ckrc20241204).

References

Brauner, N., Rovinsky, J., Moalem, M.D., 1996. Determination of the interface curvature in stratified two-phase systems by energy considerations. Int. J. Multiphas. Flow 22 (6), 1167–1185. https://doi.org/10.1016/0301-9322(96)00046-8.
Brauner, N., Moalem, M.D., Rovinsky, J., 1998. A two-fluid model for stratified flows with curved interfaces. Int. J. Multiphas. Flow 24 (6), 975–1004. https://doi.org/10.1016/S0301-9322(98)00005-6.
Chen, K., Zhang, J.R., Xu, S.Y., et al., 2025. Review of carbonated water injection as a promising technology to enhance oil recovery in the petroleum industry: Challenges and prospects. Pet. Sci. 21 (6), 4100–4118. https://doi.org/10.1016/j.petsci.2024.07.009.
Cezary, E., Paweł, S., 2024. Problems of measuring gas content in oil in a two-phase flow: A review. Energies 17 (19), 4800. https://doi.org/10.3390/en17194800.
Edomwonyi-Out, L.C., Angeli, P., 2015. Pressure drop and holdup predictions in horizontal oil-water flows for curved and wavy interfaces. Chem. Eng. Res. Des. 93 (0), 55–65. https://doi.org/10.1016/j.cherd.2014.06.009.
Garmroodi, M.R.D., Ahmadpour, A., 2020. Numerical simulation of stratified waxy crude oil and water flows across horizontal pipes in the presence of wall heating. J. Petrol. Sci. Eng. 193, 107458. https://doi.org/10.1016/j.petrol.2020.107458.
Gnielinski, V., 2009. Heat transfer coefficients for turbulent flow in concentric annular ducts. Heat. Transfer. Eng. 30 (6), 431–436. https://doi.org/10.1080/01457630802528661.
Hapanowicz, J., Polaczek, P., 2013. Convective heat transfer of a liquid dispersion system flowing in a pipe. Exp. Therm. Fluid Sci. 45, 1–7. https://doi.org/10.1016/j.expthermflusci.2012.11.007.
Hishida, M., Nagano, Y., Tagawa, M., 1986. Transport processes of heat and momentum in the wall region of turbulent pipe flow. In: International Heat Transfer Conference 8, 17–22.. https://doi.org/10.1615/IHTC8.1860.
Hong, J.J., Wang, Z.H., Wang, C., et al., 2025. Modeling of multiphase flow with the wellbore in gas-condensate reservoirs under high gas/liquid ratio conditions and field application. SPE J. 30 (3), 1301–1314. https://doi.org/10.2118/221053-PA.
Jia, S.T., Dong, C.S., 2023. Flow and heat transfer model for turbulent-laminar/turbulent gas-liquid annular flows. Appl. Therm. Eng. 219 (Part A), 119431. https://doi.org/10.1016/j.applthermaleng.2022.119431.
Jones, W.P., Launder, B.E., 1973. The calculation of low-reynolds-number phenomena with a two-equation model of turbulence. Int. J. Heat Mass Tran. 16 (6), 1119–1130. https://doi.org/10.1016/0017-9310(73)90125-7.
Karimi, H., Boostani, M., 2016. Heat transfer measurements for oil-water flow of different flow patterns in a horizontal pipe. Exp. Therm. Fluid Sci. 75, 35–42. https://doi.org/10.1016/j.expthermflusci.2016.01.007.
Kays, W.M., 1994. Turbulent prandtl number-where are we? J. Heat Tran. 116 (2), 284–295. https://doi.org/10.1115/1.2911398.
Lang, P., Auracher, H., 1996. Heat transfer to nonmiscible liquid-liquid mixtures flowing in a vertical tube. Exp. Therm. Fluid Sci. 12 (3), 364–372. https://doi.org/10.1016/0894-1777(95)00127-1.
Lam, C.K.G., Bremhorst, K., 1981. A modified form of the k-ε model for predicting wall turbulence. J. Fluid Eng. 103 (3), 456–460. https://doi.org/10.1115/1.3240815.
Li, H.Y., Yap, Y.F., Lou, J., et al., 2015a. Numerical investigation of heat transfer in three-fluid stratified flows. Int. J. Heat Mass Tran. 89, 576–587. https://doi.org/10.1016/j.ijheatmasstransfer.2015.05.083.
Li, H.Y., Yap, Y.F., Lou, J., et al., 2015b. Numerical modelling of three-fluid flow using the level-set method. Chem. Eng. Sci. 126 (1), 224–236. https://doi.org/10.1016/j.ces.2014.11.062.

Li, N.L., Chen, B., 2024. Evaluation of frictional pressure drop correlations for air-water and air-oil two-phase flow in pipeline-riser system. Pet. Sci. 21 (2), 1305–1319. https://doi.org/10.1016/j.petsci.2023.09.020.
Li, Y., He, G., Sun, L., et al., 2018. Numerical simulation of oil-water Non-Newtonian two-phase stratified wavy pipe flow coupled with heat transfer. Appl. Therm. Eng. 140 (1), 266–286. https://doi.org/10.1016/j.applthermaleng.2018.05.048.
Liu, H.S., Duan, J.M., Li, J., et al., 2022. Numerical quasi-three dimensional modeling of stratified oil-water flow in horizontal circular pipe. Ocean. Eng. 251, 111172. https://doi.org/10.1016/j.oceaneng.2022.111172.
Liu, Y., Zhang, H., Wang, S., et al., 2008. Prediction of pressure gradient and holdup in small Eötvös number liquid-liquid segregated flow. Chin. J. Chem. Eng. 16 (2), 184–191. https://doi.org/10.1016/S1004-9541(08)60060-9.
Małgorzata, S., Tadeusz, B., Katarzyna, T., et al., 2024. The effect of channel surface roughness on two-phase flow patterns: A review. Energies 17 (21), 5483. https://doi.org/10.3390/en17215483.
Newton, C.H., Masud, B., 2000. Numerical calculation of turbulent stratified gas-liquid pipe flows. Int. J. Multiphas. Flow 26 (2), 327–337. https://doi.org/10.1016/S0301-9322(99)00010-5.
Newton, C.H., Masud, B., 2001. A numerical model of stratified wavy gas-liquid pipe flow. Chem. Eng. Sci. 56 (24), 6851–6861. https://doi.org/10.1016/S0009-2509(01)00322-0.
Piroozian, A., Manan, M.A., Ismail, I., et al., 2016. Mixture temperature prediction of waxy oil-water two-phase system flowing near wax appearance temperature. Chinese. J. Chem. Eng. 24 (6), 795–802. https://doi.org/10.1016/j.cjche.2015.12.022.
Santos, D.S., Faia, P.M., Garcia, F.A.P., et al., 2019. Oil/water stratified flow in a horizontal pipe: simulated and experimental studies using EIT. J. Petrol. Sci. Eng. 174, 1179–1193. https://doi.org/10.1016/j.petrol.2018.12.002.
Somer, T.G., Bora, M., Kaymakçalan, Ö., et al., 1973. Heat transfer to an immiscible liquid mixture and between liquids in direct contact. Desalination 13 (3), 231–249. https://doi.org/10.1016/S0011-9164(00)80054-5.
Shang, W., Sarica, C., 2013. A model for temperature prediction for two-phase oil/water stratified flow. J. Energy Resour. Technol. 135 (3), 32906. https://doi.org/10.1115/1.4023931.
Sunday, N., Settar, A., Chetehouna, K., et al., 2023. Numerical modeling and parametric sensitivity analysis of heat transfer and two-phase oil and water flow characteristics in horizontal and inclined flowlines using OpenFOAM. Pet. Sci. 2, 1183–1199. https://doi.org/10.1016/j.petsci.2022.10.008.
Yang, K., Wang, Y.L., Wang, M., et al., 2023. A unified heat transfer model for gas-liquid two-phase mixing process in a rectangular channel based on steady status identification. Appl. Therm. Eng. 236 (Part B), 121612. https://doi.org/10.1016/j.applthermaleng.2023.121612.
Yin, B.T., Chen, C., Feng, K., et al., 2025. Multiphase transient flow in wellbore during shallow hydrate reservoir drilling in deep water. ACS Omega 10 (13), 13701–13714. https://doi.org/10.1021/acsomega.5c01229.
Zhang, K., Liu, X.F., Wang, D.B., et al., 2024. A review of reservoir damage during hydraulic fracturing of deep and ultra-deep reservoirs. Pet. Sci. 21 (1), 384–409. https://doi.org/10.1016/j.petsci.2023.11.017.